INTERNATIONAL ATOMIC ENERGY AGENCY
UNITED NATIONS EDUCATIONAL, SCIENTIFIC AND CULTURAL ORGANIZATION
INTERNATIONAL CENTRE FOR THEORETICAL PHYSICS
I.C.T.P., P.O. BOX 586, 34100 TRIESTE, ITALY, CABLE CENTRATOM TRIESTE

H4.SMR/453-15

TRAINING COLLEGE ON
PHYSICS AND CHARACTERIZATION
OF LASERS AND OPTICAL FIBRES

(5 February - 2 March 1990)

GAIN, ABSORPTION AND SATURATION INTENSITY
MEASUREMENTS OF AN X-RAY PREIONIZED,
DISCHARGE PUMPED Xe-Cl LASER

T. Letardi

ENEA
Centro Ricerche Energia
Roma, Frascati 00044
Italy

ISSN/0393 6333

ENEA
COMITATO NAZIONALE PER LA RICERCA E PER LO SVILUPPO
DELL'ENERGIA NUCLEARE E DELLE ENERGIE ALTERNATIVE

GAIN, ABSORPTION AND SATURATION INTENSITY MEASUREMENTS OF AN X-RAY PREIONIZED, DISCHARGE PUMPED Xe-Cl LASER

L. LETARDI, P. DI LAZZARO, G. GIORDANO, E. SABIA
ENEA - Dipartimento Tecnologie Intersettoriali di Base, Centro ricerche energia Frascati

V. BOFFA, S. BOLLANTI, T. HERMSEN
ENEA Guest

C.E. ZHENG
Shanghai Institute of Optics and Fine Mechanics and ENEA Guest

RT/TIB/87/49

Testo pervenuto nel gennaio 1988
Progetto Enea: Progetto tecnologie ottiche ed elettro-ottiche (QU)

ABSTRACT

The small signal gain and absorption coefficients of a high uniformity, X-ray preionized Xe-Cℓ laser have been measured. Their time evolution and wavelength dependence have been simultaneously detected with high resolution.

Two distinct estimates of the saturation intensity were obtained by means of a Rigrod-type analysis of the intracavity intensity and by using saturated gain measurements.

RIASSUNTO

I coefficienti di guadagno a piccolo segnale di assorbimento di un laser Xenon Cloride, preionizzato a raggi X, sono stati misurati, sia in funzione del tempo sia della lunghezza d'onda.

Inoltre sono stati ottenuti due valori per l'intensità di saturazione usando due diversi tipi di analisi di Rigrod.

I. INTRODUCTION

We present the results of a detailed experimental study of the gain characteristics of a high uniformity, X-ray preionized, self sustained discharge Xe-Cℓ laser, entirely realized at the ENEA center of Frascati.

The laser system, described in Ref. [1,2], consists of a laser cell with an active volume of about 1 liter (dimensions 3,5x3,5x80 cm^3), filled with a gas mixture of HCℓ/Xe/Ne (1:6,7:2019) at a total pressure of 4 atm. The active medium is uniformly preionized by X-rays using a 3 kA, 50 ns pulsed plasma cathode and a resonantly charged tungsten target anode. Using a plano-plano cavity a highly uniform and relatively low divergence (< 2 mrad) laser output-beam was achieved, with a pulse energy of more than 3 joule and a 150 ns pulsewidth. At an energy level of 1.5 J/pulse, the total and intrinsic efficiencies were 2,0% and 3,6% respectively [2,3].

In order to gain a deeper insight into the physical characteristics of this device, the time and spectral dependence of the small signal gain and absorption coefficients together with the saturation intensity have been investigated. Due to the intrinsic nonsaturable absorption, the extraction efficiency of excimer lasers depends on the parameters $g_o \cdot \ell$ and $\gamma = g_o/\alpha$, where g_o is the small signal gain coefficient, α is the non-saturable absorption coefficient and ℓ is the active medium length. It is therefore necessary to know the temporal evolution of these parameters in order to predict and to optimize the performance of any Rare Gas Halide laser.

The time and spectrally resolved gain and absoption measurements were performed using the frequency doubled output of a long pulse, flash pumped dye laser to probe the active medium in the wavelength range around the main laser transition lines. Thus the high resolution ($\Delta\lambda$ = 0,5 Å) spectral profile of the gain and the time evolution (resolution ΔT = 5 ns) of both the gain on the four B-X transitions and the absorption coefficients have been obtained.

Finally, two different measurements were performed to obtain an estimate of the saturation intensity. Both make use of a Rigrod analysis of the intracavity intensity at different reflectivities of the output coupler, but with the difference that in the first measurement the saturation intensity was calculated directly from the measured output intensity by solving the resulting transcendental equation, while in the second measurement the saturation intensity was obtained from the mean intracavity intensity and the measured gain of a probe beam.

Most of the measurements of g_0 and α were performed at an energy deposition rate of 200 kW/cm^3, but some were done at 250 kW/cm^3 and 350 kW/cm^3. These pumping rate density values were obtained from a numerical simulation of the discharge circuit and checked by means of a more direct method which uses the pressure jump in the laser cell during discharge [4]. All measurements of the saturation intensity refer to an energy deposition rate of 350 kW/cm^3.

The paper is organized as follows: in sect II we describe the experimental setup and give the results relative to the absorption and gain coefficient measurements, while sect III is devoted to the measurements of the saturation intensity. Final conclusions are drawn in sect IV.

II. MEASUREMENT OF THE ABSORPTION COEFFICIENT AND THE SMALL SIGNAL GAIN COEFFICIENT

Experimental setup

The intensity I_2 of a probe laser beam at the exit of an amplifying medium can be expressed in terms of the input intensity I_1 by

$$I_2 = I_1 \exp[(g_0 - \alpha)\ell] \qquad (2.1)$$

where g_0 is a function of both the wavelength and time, while α is supposed to be only time dependent in the operating wavelength region; ℓ is the active medium length. The expression (2.1) holds only for steady state amplification and if the condition for the probe beam intensity

$$I(z) \ll I_s \,, \qquad 0 \le z \le \ell \qquad (2.2)$$

is satisfied. The saturation intensity I_s is a characteristic parameter of the active medium and in our case was of the order of 1 MW/cm^2. Before every set of measurements, the fulfillment of condition (2.2) was checked through the linearity of I_2 versus I_1.

The experimental setup is drawn in Fig. 1. The Phase-R DL 1100

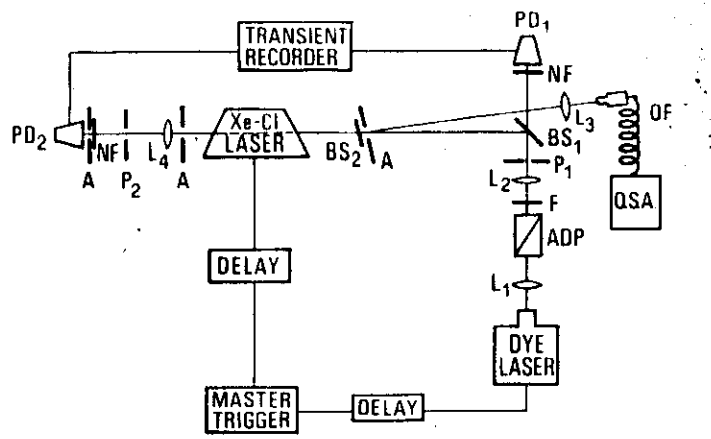

Fig. 1 Experimental layout for small signal gain and absorption coefficients measurement, where

L_1 focal length = 20 cm	PD = photodiode
L_2 focal length = 15 cm	OF = optical fiber
L_3 focal length = 10 cm	BS = beam splitter
L_4 focal length = 15 cm	F = UG11 Schott filter
P_1 = pinhole ϕ = 4 mm	NF = neutral density filters
P_2 = pinhole ϕ = 0.5 mm	A = aperture

flash-pumped dye laser used in the experiment has a pulse duration which can range from 100 to 250 ns, by changing the net gain of the active medium. A typical output pulse shape is shown in Fig. 2. The optical resonator of the dye laser includes a couple of quartz prisms to reduce the spectral width of the fundamental wavelength emission to 0.5 Å after frequency doubling, as shown in Fig. 3. Using a 5×10^{-5} mol/ℓ ethanolic solution of Rhodamine B as active medium and an ADP second harmonic crystal, the UG11 Schott filter selected output wavelength could easily be varied between 3075 Å and 3140 Å.

The small signal gain coefficient has been measured in the wavelength interval 3075 Å - 3085 Å, while the absorption coefficient has been measured only for $\lambda > 3085$ Å. As a matter of fact, for wavelengths shorter than the emission peak ($\lambda < 3080$ Å), there is a long fluorescence tail [5], primarily due to transitions originating from $v' > 1$ vibrational levels in the B electronic state, which do not permit absorption measurement.

The maximum second harmonic output energy ranged from 0.5 to 2.0 mJ, depending on the operating wavelength. After the spatial filter P_1 (see Fig. 1), a

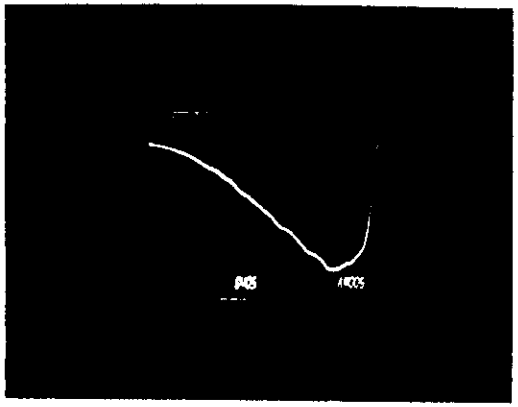

Fig. 2 Dye laser pulse temporal evolution

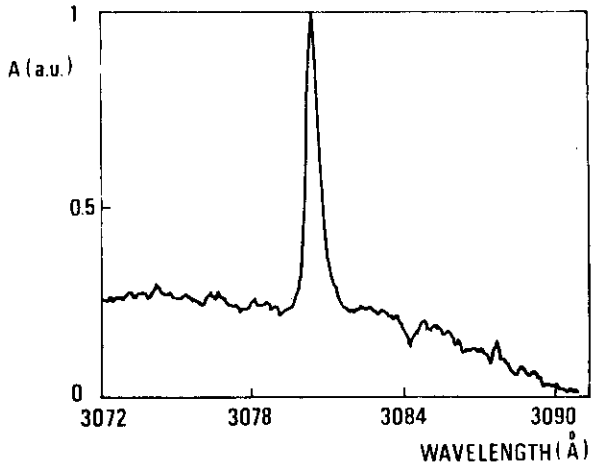

Fig. 3 Second harmonic dye laser single pulse spectrum

collimated laser beam with a 4 mm spot diameter was available for the measurements. The probe laser beam power and wavelength were monitored by means of an ITT FW114A photodiode and an optical spectrum analyzer (OSA) respectively. The OSA was used in conjunction with a 0,75 m spectrometer with a 3600 rows/mm grating, (overall spectral resolution: $\Delta\lambda$=0.12 Å) and an optical fiber allowed the beam handling (see Fig. 1). Neutral density filters were inserted at the entrance of the Xe-Cℓ medium in order to limit the probe beam intensity and thus ensuring the gain linearity. An optical filtering system behind the Xe-Cℓ target, composed of a lens and a pinhole, increased the signal to noise ratio, where the background noise derived essentially from the Xe-Cℓ fluorescence. Finally the amplified beam was monitored by means of a second ITT photodiode after attenuation to ensure that the detector working point was far away from saturation.

Data acquisition and elaboration

The hardware of the data acquisition consisted of a PDP 11/60 calculator, with standard Camac and a IEEE 488 Interfaces (see Fig. 4). The latter allowed the use of a dual channel digitizer Tektronix 7612D to record both the probe and reference pulses with a resolution of 5 ns.With the same waveform digitizer it was possible to observe the sustainer voltage, so that the delay between the discharge breakdown and the dye laser pulse could be determined. The Camac

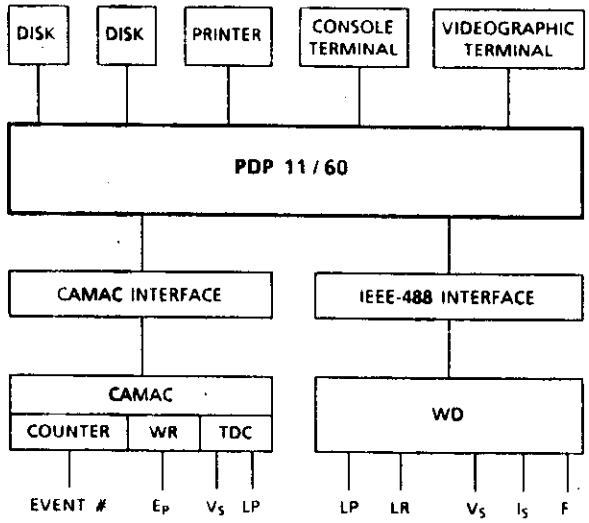

Fig. 4 Data acquisition system:
- E_p = energy transferred to the gas during the discharge
- V_s = discharge voltage
- I_s = discharge current
- F = fluorescence
- LP = dye laser probe pulse from PD2
- LR = dye laser reference pulse from PD1
- WD = dual channel digiter Tektronix 7612 D
- WR = fast pressure transducer BHL 4101-00
- TDC = time-to-digital converter

allowed the measurement of the transient pressure increase in the active medium (by means of a BHL 4101-00 Bell-Howell fast pressure transducer) which can be related to the pumping energy transferred to the gas [4].

In writing the software for data storage and elaboration special attention was devoted to the problem of the time correlation between the reference and the probe pulses. We decided to adopt the following method for the absorption coefficient. First the mixture without discharge was probed. In this case, neglecting any absorption by the Ne-Xe-HCℓ mixture, the ratio R_1, channel for channel, between the probe pulse and the reference pulse should be constant. R_1 and its error bar (due to instrument noise and digitalization) were found *shifting* the pulses until a least square fit of the various ratios gave the smallest variation with respect to a constant. Next, the mixture with a discharge was probed, and the shifting procedure was repeated, looking now for the smallest variation with an arbitrary straight line. In this way the time dependent ratio $R_2(t)$ and its corresponding error bars were obtained. Indeed, the assumption that the overall absorption coefficient changes almost linearly over the 150 ns time duration of the probe pulse seems to be reasonably correct. The time dependent absorption coefficient α was then calculated from Eq. (2.1) by the formula $\alpha(t) = \ell n(R_2(t)/R_1)/\ell$.

Essentially the same scheme was used to calculate the time dependent small signal gain coefficient g_0 around the main laser transition lines. The only difference was that, due to the nonlinear behavior of g_0 over the time duration of the probe pulse, the correlation between the probe and reference pulse in the case of discharge was determined by using the measured delay between the pulses without discharge.

The absorption coefficient α

The measured time dependence of the absorption coefficient for three different wavelengths λ = 3110 Å, 3125 Å and 3140 Å is reported in Figs 5, 6, 7 respectively.

The first was chosen because of the expected negligible gain at on this wavelength [6]. Corkum and Taylor [7] assume that the absorption coefficients at 311 nm and 308 nm are the same due to the broad band absorption spectra of the species (e.g. Xe^*_2, $C\ell$, $Xe_2C\ell$, Ne^{**}) which are thought to be important in the Ne based $XeC\ell$ laser mixture during discharge [8]. However, we preferred to use the measurement results on wavelength λ=312,5 nm, because the absorption measurement on 311 nm seems to be rather disturbed leading to an unlikely high value for the ratio $g_0/\alpha > 50$ on the laser transition line. This choice is also supported by the small difference between the absorption curves on 312,5 nm and 314,0 nm, as can be seen from the figures, which seems to confirm the broad band absorption around the laser transition lines.

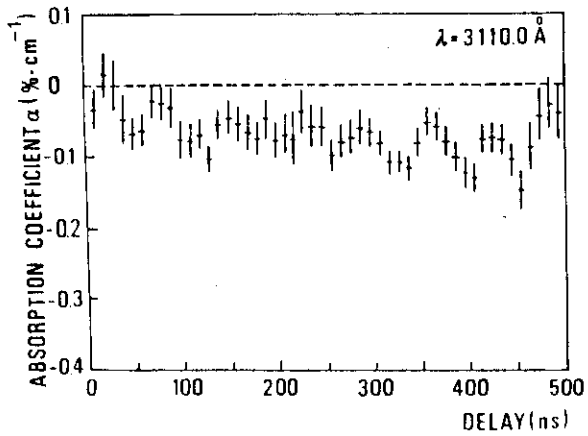

Fig. 5 Absorption coefficient α vs time for λ = 3110 Å

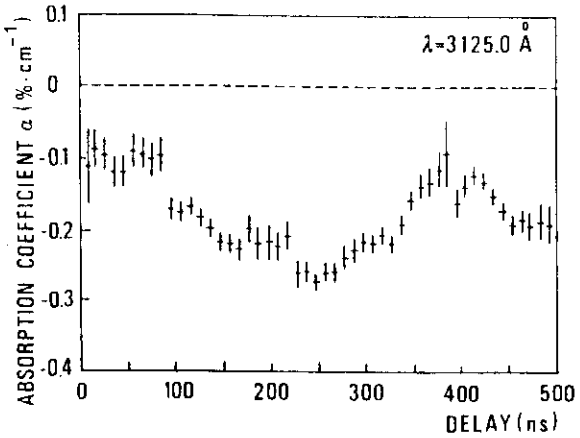

Fig. 6 Absorption coefficient α vs time for λ = 3125 Å

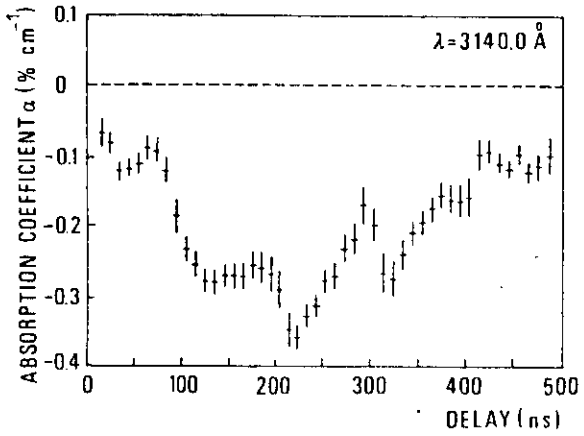

Fig. 7 Absorption coefficient α vs time for λ = 3140 Å

A time interval of about 500 ns was covered varying the delay between the discharge breakdown and the probe pulse. No larger times were considered because it has been observed that the measurements would be seriously disturbed because of the formation of inhomogeneities in the refractive index of

the mixture after about 500 ns, corresponding to the base width duration of the current pulse [7].

As a result of these measurements, we calculated a peak value of the absorption coefficient a = 0,27 ± 0,01%/cm at wavelength λ = 312,5 nm and with a power deposition rate of 200 kW/cm^3.

As evident from the Figs (5-7) the absorption reaches a maximum value after the peak power deposition, in a similar way as in previously published absorption measurements using e-beam excitation [9] and UV preionization [7], both at a much higher power deposition level (~ 3 GW/ℓ). In particular, the two-component behavior of the absorption (see Figs 6 and 7) may be due, according to Ref. 7, to Xe^+_2 in the high E/P region and to Xe^*_2 in the afterglow. This conjecture is supported by the different formation onset times of the two mentioned species [10].

The small signal gain coefficient g_o

Figures 8, 9, 10 and 11 show the measurement results of the time behavior after the discharge of the net gain coefficient $g_o - a$ for different wavelengths

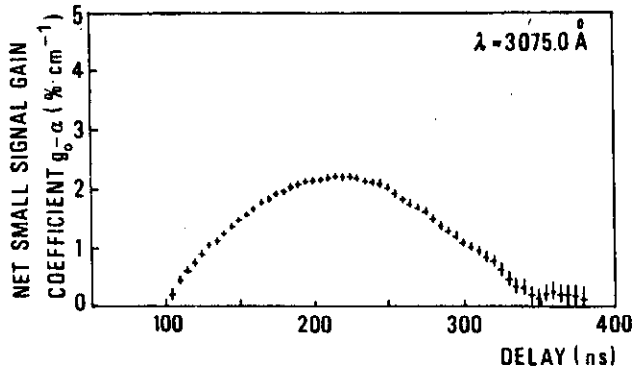

Fig. 8 Net small signal gain coefficient $g_o - a$ vs time for λ = 3075 Å

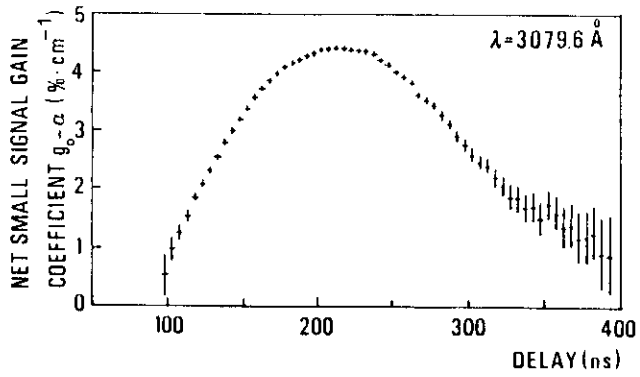

Fig. 9 Net small signal gain coefficient $g_o - a$ vs time for λ = 3079.6 Å

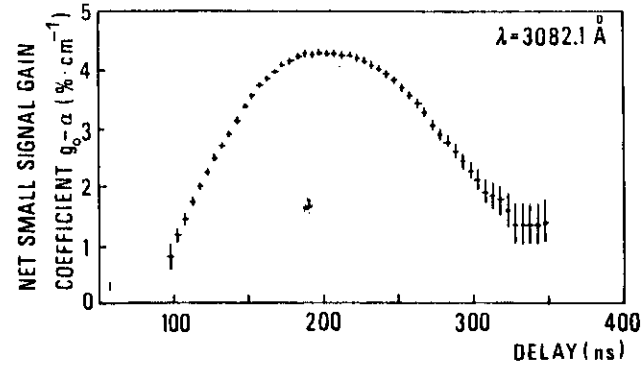

Fig. 10 Net small signal gain coefficient $g_o - a$ vs time for λ = 3082 Å

in the interval 3075 - 3085 Å around the laser transition lines, at a pumping rate deposition of 200 kW/cm^3. A maximum value of g_o = 4.7%/cm was obtained for λ = 3079.6 Å (corresponding to the main laser transition line) and for a delay time of about 230 ns. Using the measured peak value of the absorption coefficient, we calculate a gain to loss ratio g_o/a = 18±1 at the peak of the gain.

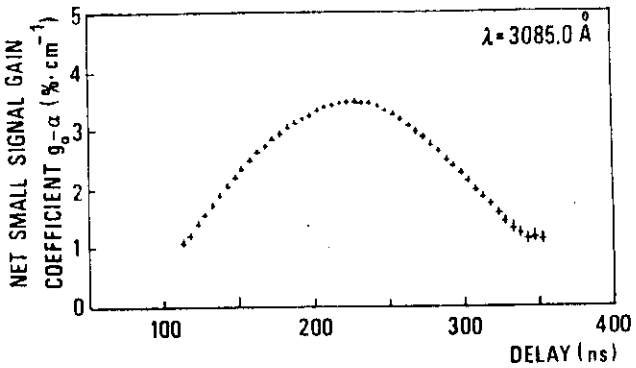

Fig. 11 Net small signal gain coefficient $g_o - \alpha$ vs time, for λ = 3085 Å

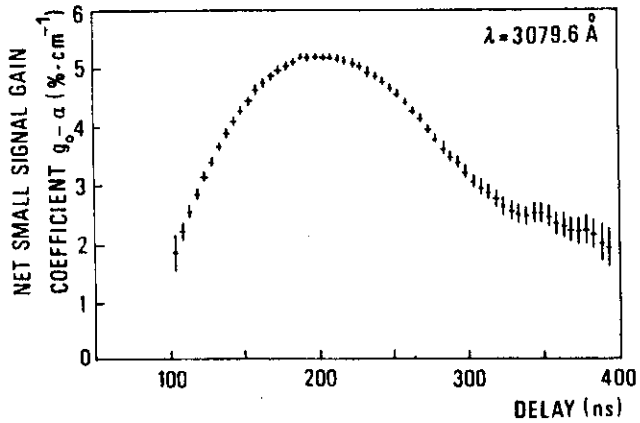

Fig. 12 Net small signal gain coefficient $g_o - \alpha$ vs time, for λ = 3079.6 and a pumping rate density of 250 kW/cm^3

The gain and absorption coefficients measurement was repeated at an higher pumping rate density of 250 kW/cm^3, in order to check the pumping dependence of the coefficient $\gamma = g_o/\alpha$. Figure 12 and 13 show the time histories of the small signal gain at the main transition line and of the absorption coefficient at λ=3125 Å respectively. Both time behaviors resemble that of the

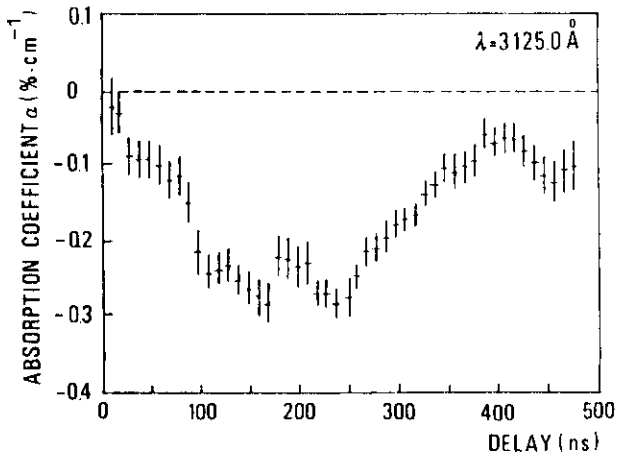

Fig. 13 Absorption coefficient α vs time at λ = 3125 Å for a pumping rate density of 250 kW/cm^3

corresponding ones at lower deposition rate (Figs 6 and 9) and the resulting factor $\gamma = g_o/\alpha = 20 \pm 2$ is the same (within the error bars) with respect to the above reported γ value at 200 kW/cm^3. This seems to be in agreement with the experimental results reported in Ref. 9.

Figure 14 shows the net small signal gain coefficient as a function of the wavelength for a fixed time delay of 230 ns. The corresponding measured XeCℓ emission spectral profile reported in Fig. 15 is a type of multimaximum having peaks at 307.6 nm, 307.9 nm, 308.2 nm and 308.4 nm, confirming that the XeCℓ laser takes place in the form of the bound-bound transition, as expected theoretically [11]. To our knowledge it is the first time that the gain profile of all four B-X transition lines have been clearly resolved for the Ne based XeCℓ laser mixture (for He/Xe/Cℓ see Ref. 12). It should be mentioned that no attempt has been made to correct this gain curve for the finite bandwidth of the probe beam, which would probably result in more pronounced difference between the minima and maxima (cfr Figs 14 and 15).

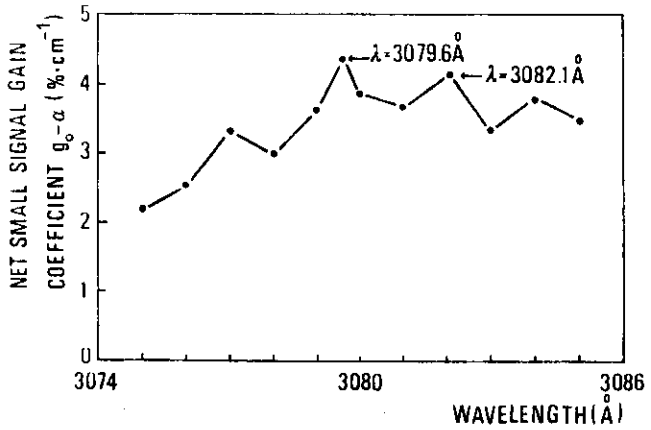

Fig. 14 Net small signal gain coefficient $g_o - \alpha$ vs wavelength λ, for delay time of 230 ns and a pumping rate density of 200 kW/cm^3

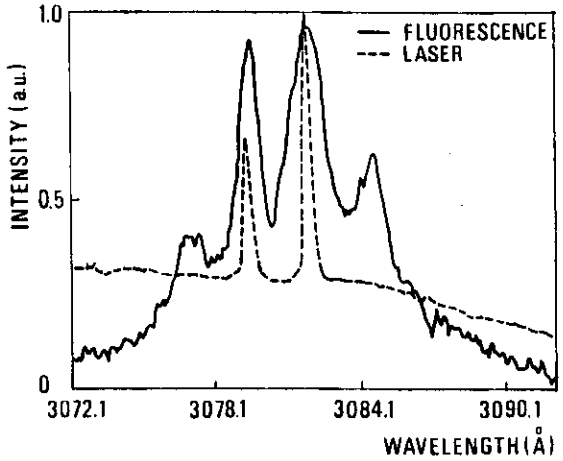

Fig. 15 Emission spectral profile of XeCl active medium

Finally, in Fig. 16 we show the peak small signal gain coefficient for different energy deposition rates in the laser cell.

III. MEASUREMENTS OF THE SATURATION INTENSITY

To obtain an estimate of the saturation intensity of the mixture, two different experimental measurements were performed. The first makes use of a Rigrod type analysis of the laser output intensity of a plano-plano cavity, as a function of the mirror reflectivities and the saturation intensity [13]. Strictly

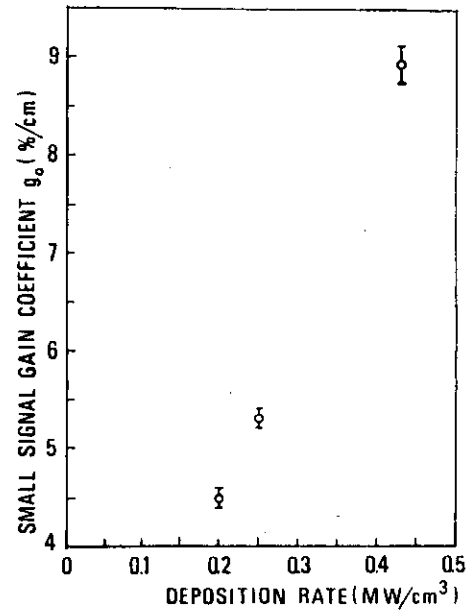

Fig. 16 Small signal gain coefficient g_o vs energy deposition rate in the XeCl active medium

speaking this method is only valid under stationary conditions, but one can show (see Appendix A) that for our experimental conditions the steady state approximation is well satisfied. Using a geometrical approximation one may write for the right and left travelling intensities $I_+(z)$ and $I_-(z)$

$$\frac{1}{I_+}\frac{dI_+}{dz} = \frac{g_0}{1+\frac{I_+}{I_s}+\frac{I_-}{I_s}} - a = -\frac{1}{I_-}\frac{dI_-}{dz} \qquad (3.1)$$

with the boundary conditions

$$I_-(L) = I_+(L)\, R_2\, T_f^2$$

$$I_+(0) = I_-(0)\, R_1\, T_f^2 \qquad (3.2)$$

R_1 and R_2 are the reflectivities of the back and the output mirror respectively, and T_f the transmittance of the quartz-windows in the gas chamber. Equation (3.1) may be integrated to obtain a transcendental equation in the variable $\delta = I_+ I_-/I_s^2$. Solving this equation for δ as a function of the parameters R_1, R_2, T_f, g_0 and a, one may calculate the saturation intensity from the measured intensity I_e at the exit of mirror M_2. To determine the peak output intensity, both the laser pulse shape and the total pulse energy were measured.

The values of the parameters used were

R_1 = 98%

T_f = 99%

g_0 = 8.9 ± 0.2%/cm

a = 1.4 ± 0.3%/cm

TABLE I: Results of first saturation intensity measurement

R_2(%)	I_e (Mw/cm^2)	I_s (Mw/cm^2)	$\langle I_s \rangle$ (Mw/cm^2)
10	1.0 ± 0.2	0.4 $^{+0.2}_{-0.1}$	
23	1.0 ± 0.2	0.5 $^{+0.2}_{-0.2}$	0.5 $^{+0.3}_{-0.2}$
84	0.26 ± 0.06	0.6 $^{+0.4}_{-0.2}$	

while for R_2 three values were taken, namely, R_2=10%, 23%, and 84%. The higher value of the peak small signal gain coefficient with respect to the earlier measured g_0 is due to the higher pumping rate deposition in this case (350 kW/cm^3). This implies a correspondingly higher absorption coefficient assuming a constant ratio g_0/a [9]. The value of the effective absorption coefficient was obtained by taking the sum of the intrinsic absorption coefficient (0.5 ± 0.1%/cm) and the estimated loss due to diffraction (0.9 ± 0.2%/cm).

From these measurements three values for the saturation intensity were calculated (see Table I) with a mean value of

$$\langle I_s \rangle = 0.5 \begin{cases} +0.3 \\ \\ -0.2 \end{cases} \text{MW/cm}^2 \qquad (3.3)$$

The error bars were calculated by finding the maximum and minimum values of I_s, varying the parameters a, g_0, and I_e within their error bars.

The second method uses the intracavity intensity dependence of the gain of a probe beam. Indeed, for the propagation of the probe beam with a sufficiently low intensity I (i.e. $I << I_c$) we may write:

$$\frac{dI}{dz} = \left(\frac{g_0}{1 + I_c(z)/I_s} - a \right) I \qquad (3.4)$$

The intracavity intensity $I_c(z)$ depends on the longitudinal coordinate z. However, it can be shown (see Appendix B) that the error made in Eq. (3.4) by taking its mean value over the cavity length is small, and hence the equation may be integrated to give for the amplified probe beam the following expression:

$$I_{out} = I_{in} \exp\left[\left(\frac{g_0}{1 + \langle I_c \rangle / I_s} - a \right) \ell \right] = I_{in} \exp(g \cdot \ell) \qquad (3.5)$$

where g is the net gain coefficient of the probe beam. Using a modified Rigrod analysis [14] one may express the mean intracavity intensity $\langle I_c \rangle$ in terms of the intensitiy I_e at the output coupling mirror M_2:

$$\langle I_c \rangle = - \frac{\left(1 - \sqrt{R_1 \cdot R_2 \cdot T_\ell^4} \right) \left(\sqrt{R_1} + \sqrt{R_2} \right)}{(1 - R_2) T_1 \cdot \sqrt{R_1} \cdot \ln \sqrt{(R_1 \cdot R_2 \cdot T_\ell^4)}} \cdot I_e \qquad (3.6)$$

In this way, by measuring the amplified probe beam intensity I_{out} and the laser intensity I_e at the exit of mirror M_2, one may calculate the saturation intensity.

TABLE II: Results of second saturation intensity measurement

R_2(%)	I_e (Mw/cm^2)	g(%/cm)	I_s (Mw/cm^2)	$\langle I_s \rangle$ (Mw/cm^2)
10	1.0 ± 0.2	4.9 ± 0.3	1.4 $^{+0.7}_{-0.5}$	1.2 $^{+0.6}_{-0.4}$
23	1.0 ± 0.2	3.7 ± 0.4	1.2 $^{+0.7}_{-0.4}$	
84	0.26 ± 0.06	2.23 ± 0.05	1.3 $^{+0.5}_{-0.4}$	

Of course, this method depends heavily on the technical possibility of separating the amplified probe beam from the much larger overall background laser intensity. This has been achieved elegantly by means of the Brewster angle quartz windows W_1 and W_2.

The experimental set up is schematically drawn in Fig. 17. The probe beam was taken from a Lambda Physik EMG50 XeCl laser with 17 ns (FWHM) pulse duration, which was attenuated (filter A), recollimated (lenses L_1 and L_2) and spatially filtered (pinhole PH) before entering the laser cell. The other experimental conditions (mirrors reflectivity, pumping rate, etc.) were left unchanged with respect to the first measurement.

Due to the different polarizations induced by W_1 and W_2 the probe beam and the intracavity e.m. field are split at window W_2, after which the gain is measured by photodiode PD1.

The results of the measurements are shown in Table II and we calculated a

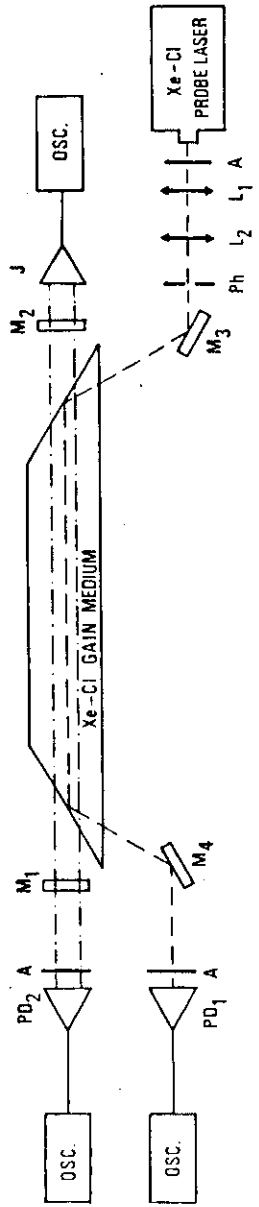

Fig. 17 Experimental setup for the second measurement of the saturation intensity (see text)
M_1 = cavity back mirror, L_2 = lens (f=25 cm)
reflectivity 99%
M_2 = cavity front mirror
M_3 = mirror
M_4 = mirror
A = neutral density filters
L_1 = lens (f=50 cm)
Ph = spatial filter
J = joule meter Gentec ED-1000
PD_1 = reference photodiode ITT, FW-114A
PD_2 = signal photodiode ITT, FW-114A

mean value of the saturation intensity of

$$\langle I_s \rangle = 1.2 \begin{cases} +0.6 \\ -0.4 \end{cases} \text{ MW/cm}^2 \qquad (3.7)$$

Again, the error bars were calculated by finding the maximum variation in I_s, changing the parameters within their range.

IV. CONCLUSIONS

The absorption coefficient α and the small signal gain coefficient g_0 have been measured, both as a function of the time elapsed after discharge breakdown, and g_0 as a function of the wavelength. It should be noted that the time dependence of the absorption is rather similar to that of the small signal gain coefficient g_o (width, onset time, peak time) leading to an approximately constant ratio g_o/α with time.

Two different measurements of the saturation intensity were performed leading to the values 0.5 Mw/cm^2 and 1.2 Mw/cm^2 respectively. However, taking into account the rather large error bars (see 3.3 and 3.7) these results are not really in contradiction but rather reflect the considerable difficulty in measuring this quantity. These considerations are, on the other hand, largely stated by the wide range of saturation intensity measured values, also for apparently similar experimental conditions [7, 9, 15, 16].

ACKNOWLEDGEMENT

We thank T. Mazzinghi and M. Vannini of the Institute of Quantum Electronics in Florence, for many stimulating discussions.

APPENDIX A

We will show the validity of the steady state approximation under the experimental conditions in the first measurement of the saturation intensity.

Let us begin with an estimate of the spontaneous emission power density I_0:

$$I_0 = g_0 I_s \cdot \left(\frac{\Phi \cdot \ell}{4\cdot\pi}\right) = 16.1\ \mathrm{W/cm^2} \qquad (A.1)$$

where ℓ = 80 cm is the active medium length, ϕ = (discharge cross section)/ℓ^2= $5.8\cdot10^{-4}$ is a geometrical factor, g_0=8.9% cm^{-1} and I_s=0.5 MW/cm^2 are the values relative to the first measurement of the saturation intensity.

The active medium length L needed to saturate the laser intensity can then be calculated from the equation

$$I_s = I_0 \cdot \exp[(g_0 - a)\cdot L] \qquad (A.2)$$

which gives, (using the measured values of g_0,a and I_s =0.5 MW/cm^2), L=107 cm, corresponding to ~ 1.3 passes in the active medium. With a mirror spacing of 150 cm, saturation is reached after about 7 ns. The measured fluorescence halfwidth was about 100 ns, so that saturation is obtained well before the fluorescence peak.

APPENDIX B

We will calculate the correction term for the saturation intensity if the intracavity intensity, instead of being approximated by its mean value, is taken to be linearly varying with the longitudinal coordinate in Eq. (3.4).

Thus taking $I_c(z)$ of the form

$$I_c(z) = (1-\delta) I_c + 2\delta I_c z/L \qquad (B.1)$$

and inserting this in the RHS of Eq. (3.4), one may integrate the equation to give for the gain g of the probe beam

$$g = \frac{g_0 \cdot x}{2\delta} \log\left(1 + \frac{2\delta}{x+1-\delta}\right) - a \qquad (B.2)$$

where $x=I_s/I_c$. The parameters I_c and δ may be calculated in terms of the reflectivities R_1 and R_2, the transmittance T_f, and the measured laser intensity I_e, by fitting the nearly exponential intracavity intensity with a straight line. Using Eq. (B.2) we may write a series expansion of x (and thus I_s) in the (small) parameter δ:

$$I_s \simeq \frac{g+a}{g_0-(g+a)} I_c - \frac{g+a}{2g_0}\delta^2 I_c = I_s^0 + I_s^{corr} \qquad (B.3)$$

where g is the net gain coefficient of the probe beam. Inserting the values of the parameters in the second measurement of I_s, the correction term was less than 2% and thus the mean intracavity intensity is the significant parameter.

REFERENCES

[1] A. De Angelis, E. Fiorentino, G.Giordano, T. Letardi, E. Sabia and M. Vannini, *High Uniformity X-ray Preionized Discharge XeCℓ Laser*, Proc. of the Int. Conf. on Lasers 84, Eds K.M. Corcoran, D.M. Sullivan, W.C. Stwalley (STS Press, Mclean VA 1985) pp. 606-611.

[2] T. Letardi, S. Bollanti, A. De Angelis, P. Di Lazzaro, I. Giabbai, G. Giordano, and E. Sabia, *Characterization of High Uniformity, X-ray Preionized XeCℓ Laser*, to be published in Nuovo Cimento D.

[3] V. Boffa, S. Bollanti, P. Di Lazzaro, G. Giordano, T. Hermsen, T. Letardi and E. Sabia, *Study of a High Energy, X-ray Preionized Discharge XeCℓ Laser*, 1986 European Conference on Optics, Optical Systems and Applications, Eds S. Sottini, S. Trigari, Proc. SPIE 701 (1987). pp. 158-165.

[4] E. Fiorentino, T. Letardi, A. Marino, E. Sabia, and M. Vannini, *Electron-beam Sustained Discharge XeCℓ Laser*, Laser and Particle Beams, **3**, pp. 319-345, 1985.

[5] J.B. Laudenlager, T.S. Pacala, I.S. Mcdermid, *Scanning, Tunable XeCℓ Laser Characteristics and Application to Lic Detection of OH*, CLEO 81, post deadline paper.

[6] J. Tellinghuisen, J.M. Hoffman, G.C. Tisone, A.K. Hays, *Spectroscopic Studies of Diatomic Noble Gas Halides. Analysis of Spontaneous and Stimulated Emission from XeCℓ*, J. Chem. Phys. **64**, pp. 2484-2490, 1976.

[7] P.B. Corkum, R.S. Taylor, *Picosecond Amplification and Kinetic Studies of XeCℓ*, IEEE J. Quantum Electron. **QE-18**, pp. 1962-1975, 1982;
R.S. Taylor, P.B. Corkum, S. Watanabe, K.E. Leopold and A.J. Alcock *Time-Dependent Gain and Absorption in a 5 J, UV Preionized XeCℓ Laser*, IEEE J. Quantum Electron **QE-19**, pp. 416-425, 1983.

[8] A. Mandl, *Electron Photo Detachment Cross Sections of Cl⁻ and Br⁻*, Phys. Rev. **A14**, pp. 345-348, 1976.
W.R. Wadt, P.J. Hay, *Electronic States of Ar_2F and Kr_2F*, J. Chem. Phys. **68**, pp. 3850-3863,1978.
W.R. Wadt, *The Electronic States of Ne^*_2, Kr^*_2, and Xe^*_2 II Absorption Cross Sections for the $I(1/2)u \rightarrow I(3/2)g$, $I(1/2)g \rightarrow 2(1/2)g$ Transitions*, J. Chem. Phys. **73**, pp. 3915-3926, 1980.
C. Duzy, H.A. Hyman, *Photoionization of Excited Rare-Gas Atoms*, Phys. Rev. **A22**, pp. 1878-1883, 1980.
A. Gevaudan, B.L. Fontaine, B.M. Forestier, M.L. Sentisin, *Modelling of the X-Ray Preionized XeCl Self-Sustained Discharge Laser*, Gas Flow and Chemical Lasers, Ed S. Rosenwaks (Springer Verlag, Berlin 1987) pp. 118-124.

[9] G.C. Tisone and J.M. Hoffman, *Study of the XeCℓ Laser Pumped by a High Intensity Electron Beam*, IEEE J. Quantum Electron., **QE-18**, pp. 1008-1020, 1982.

[10] L.A. Levin, S.E. Moody, E.L. Klosterman, R.E. Center, J.J. Ewing, *Kinetic Model for Long-Pulse XeCl Laser Performance*, IEEE J. Quantum Electron., **QE-17**, pp. 2282-2289, 1981.

[11] P.J. Hay, T.H. Dunning, *The Covalent and Ionic States of the Xenon Halides*, J. Chem. Phys., **69**, pp. 2209-2220, 1978.

[12] A. Takahashi, M. Sumi and M. Maeda, *A Simple Tunable Short Pulse XeCℓ Laser with High Spectral Brightness*, Opt. Commun., **55**, pp. 193 196, 1985.

[13] W.W. Rigrod, *Saturation Effects in High Gain Lasers*, J. Appl. Phys., **36** pp. 2487 2490, 1965.

[14] W.C. Marlow, *Approximate Lasing Condition*, J. Appl. Phys., **41**, pp. 4019-4022, 1970.
W.W Rigrod, *Homogeneously Broadned CW Lasers with Uniform Distributed Loss*, IEEE J. Quantum Electron., **QE 14**, pp. 377 381, 1978.

[15] R.S. Taylor, A.J. Alcock, K.E. Leopold, *Electrical and Gain Characteristics of a Simple Compact XeCl Laser*, Opt. Commun., **31**, pp. 197-202, 1979.

[16] J.H. Glowing, G. Arjaualingam, P.P. Sorokin, J.E. Rothenberg, *Amplification of 350 fs Pulses in XeCl Excimer Gain Modules*, Opt. Lett., **11**, pp. 79-81, 1986.

[17] C.A. Brau, *Rare Gas Halogen Excimers*, in Excimer Lasers, Ed C.K. Rhodes (Springer, Berlin 1983) pp. 87-90.